Thermodynamic approach to glass-forming ability of water-quenched Pd-P-based and $Pt_{60}Ni_{15}P_{25}$ bulk metallic glasses

O. Haruyama,[1] T. Watanabe,[1] K. Yuki,[1] M. Horiuchi,[1] H. Kato,[2] and N. Nishiyama[3]
[1]*Faculty of Science and Technology, Tokyo University of Science, Noda 278-8510, Japan*
[2]*Institute of Materials Research, Tohoku University, Sendai 980-8577, Japan*
[3]*RIMCOF Tohoku University Laboratory, The Materials Process Technology Center, Sendai 980-8577, Japan*
(Received 25 May 2010; revised manuscript received 26 October 2010; published 14 February 2011)

Despite its importance, a thermodynamic approach to determining the glass-forming ability (GFA) of bulk metallic glass (BMG) remains a goal to be achieved. We examined the GFA of water-quenched Pd-P-based and $Pt_{60}Ni_{15}P_{25}$ BMG's in which their molten alloys were sufficiently treated with a dehydrated B_2O_3 flux prior to and during quenching to room temperature. This allowed us to envisage the applicability of the classical steady-state homogeneous nucleation theory because the suppression of heterogeneous nucleation worked effectively. GFA was examined by comparing the critical cooling rate R_c^h for glass formation with the maximum diameter $d_{\max}$ of glass. To calculate R_c^h, the homogeneous nucleation rate $I_{ss}(T)$, and the growth rate $u_c(T)$ were estimated as functions of the undercooling temperature of molten alloys. Then, the free energy difference $\Delta G_{L-x}(T)$ between the liquid and crystalline phases, and the viscosity $\eta(T)$ of the liquid were experimentally determined while the surface energy $\sigma_{sL}(T)$ at the liquid-nucleus interface was estimated by calculation. The $d_{\max}$ of rod BMG's correlated strongly to R_c^h through the relation $R_c^h \approx d_{\max}^{-3}/10\ \mathrm{mm^3\ Ks^{-1}}$.

DOI: 10.1103/PhysRevB.83.064201 PACS number(s): 65.60.+a, 61.43.Dq, 81.05.Kf, 82.60.Nh

I. INTRODUCTION

The study of the glass-forming ability (GFA) of bulk metallic glass (BMG) is one of the most interesting fields and thus has attracted great interest among many researchers. Empirical consideration about GFA has often been taken in terms of the reduced glass transition temperature T_{rg} $[=T_g/T_l]$ and/or the γ parameter[1] $[=T_x/(T_g+T_l)]$, where T_g, T_x, T_m, and T_l are the calorimetric glass transition temperature, crystallization temperature, melting temperature, and liquidus temperature, respectively. These parameters are effective measures for explaining the GFA of a type of BMG, but they do not provide a clear physical significance of the GFA. Recently, Senkov[2] has proposed the use of the F_1 parameter to quantify the GFA of BMG's, which is defined using T_{rg} and the fragility m and is given by

$$F_1 = 2\left[\frac{m}{16}\left(\frac{1}{T_{rg}}-1\right)+2\right]^{-1}, \tag{1}$$

where m is defined by the viscosity η and a scaling glass transition temperature T_g^*, which gives a viscosity of 10^{12} Pa·s. The fragility is expressed as

$$m = \left.\frac{\partial \log_{10}\eta(T)}{\partial(T_g^*/T)}\right|_{T=T_g^*}. \tag{2}$$

It gives the slope of the curve at $T=T_g^*$ when $\eta(T)$ is described as functions of T_g^*/T. This approach emphasized the strong correlation between GFA and liquid fragility. Senkov also found that the critical cooling rate R_c for glass-formation decays exponentially with the F_1 parameter. Regarding the thermodynamic approach to determining the GFA of recently developed BMG's, several researchers have postulated the importance of the Gibbs free-energy difference[3–5] $\Delta G_{L-x}(T)$ between a liquid and its crystalline counterpart. Jiang *et al.*[4] have reported that there is a close correlation between the GFA of many Zr-based BMG's and their $\Delta G_{L-x}(T)$. $\Delta G_{L-x}(T)$ is a dominant factor in determining the driving force for crystallization in liquids. However, there are other factors that affect the kinetics of crystallization in liquids. Thus, it will be crucial to quantitatively discuss the reason why the $\Delta G_{L-x}(T)$ plays a special role in suppressing the nucleation and growth of crystal nuclei during the vitrification of molten alloys. Quaternary Pd-Cu-Ni-P alloys are a system presenting a remarkable GFA, as good as that of Zr-based metallic glasses. Nishiyama and Inoue[6] reported that $Pd_{42.5}Cu_{30}Ni_{7.5}P_{20}$ BMG shows an extremely low critical cooling rate, 0.067 K/s, for glass formation and concluded that the origin of high GFA is the low nucleation ($\approx 10^9\ \mathrm{m^{-3}\ s^{-1}}$) and growth ($\approx 10^{-7}\ \mathrm{ms^{-1}}$) rates. Shen and Schwarz[7] found that the heterogeneous nucleation rate is significantly decreased after cyclic B_2O_3 flux treatments of $Pd_{43.2}Cu_{28}Ni_{8.8}P_{20}$ molten alloy, and that the critical cooling rate for glass formation reaches a quite low value, 0.005 K/s. This observation suggests strongly that the Pd-Cu-Ni-P alloy system intrinsically possesses a significant GFA if the heterogeneous nucleation is effectively depressed. Several Pd-P- and Pt-P-based BMG's can be prepared easily by the water-quenching technique[8–10] with a B_2O_3 flux. Among all such BMG's, it is not yet clarified why quaternary Pd-Cu-Ni-P BMG exhibits an extraordinarily high GFA. The B_2O_3 flux intervenes effectively with the direct contact between the melt and the wall of the container and the vacuum environment. Drehman and Greer[11] examined the crystallization kinetics of a $Pd_{40}Ni_{40}P_{20}$ BMG from a thermodynamic point of view, and they concluded that this glass system could be vitrified at a critical cooling rate as low as 10^{-3} K/s if the heterogeneous nucleation sites were appropriately taken out. Later, Kui *et al.*[12] obtained a $Pd_{40}Ni_{40}P_{20}$ BMG ($d_{\max} \approx 10$ mm) with a dehydrated B_2O_3 flux and predicted that the homogenous steady-state nucleation rate may be less than $10^5\ \mathrm{m^{-3}\ s^{-1}}$. Cheng *et al.*[13] have calculated the relaxation time τ_α of the α-relaxation process in several Cu-Zr binary molten

alloys over a wide temperature range from equilibrium liquid temperatures down to supercooled liquid temperatures near T_g. They reported that $\tau_\alpha \approx 10^{-8}$ s near T_g. This value is much shorter than the time required for water quenching, which is roughly estimated to be a few seconds. This result ensures the thermodynamic consideration about the vitrification process of molten alloys in water quenching because the rate of atomic rearrangement at each temperature should keep up with the speed of temperature variation.

In the present study, a material's "glass-forming ability" was estimated with the maximum size $d_{\max}$ of glass sample formed. The glass samples were carefully produced under the condition that the heterogeneous nucleation and the growth mechanism did not work effectively. We estimated the homogeneous nucleation rate $I_{ss}(T)$ and the growth rate $u_c(T)$ for representative Pd-P- and Pt-P-based BMG's over a range from T_m to a temperature just below T_g.$I_{ss}(T)$ and $u_c(T)$ were estimated from the free-energy difference $\Delta G_{L-x}(T)$, the interfacial free energy between the nucleus and the liquid σ_{sl} and the viscosity $\eta(T)$. Then both the viscosity and free-energy difference were determined experimentally, while the interfacial free energy was obtained by calculation. Next, using $I_{ss}(T)$ and $u_c(T)$, the critical cooling rate R_c^h of glass formation was calculated under the assumption that a homogeneous nucleation process worked dominantly in the vitrification of molten alloys. After that, the sequence of the order of R_c^h values was compared with the maximum diameter $d_{\max}$ of the glass sample to determine the order of the GFA among all the glasses.

II. EXPERIMENTAL

Master alloys with compositions of $Pd_{40}Ni_{40}P_{20}$, $Pd_{40}Cu_{40}P_{20}$, $Pd_{46}Cu_{35.5}P_{18.5}$, $Pt_{60}Ni_{15}P_{25}$, $Pd_{42.5}Cu_{30}Ni_{7.5}P_{20}$, and $Pd_{43}Cu_{27}Ni_{10}P_{20}$ were prepared by sintering Pd (99.95 at%), Pt (99.95 at%), Cu (99.99 at%), Ni (99.993 at%), and P (99.9999 at%) at 1473 K for 8 hr in vacuum-sealed quartz tubes. After sintering, each alloy was remelted in a quartz tube and cooled to room temperature to ensure the homogeneity of the composition. This operation was repeated two times. After being homogenized, the alloy was fluxed with a dehydrated B_2O_3 by holding the melt at 1300 K for 8 hr to remove any phosphorous oxides, which are considered to become dominant heterogeneous nucleation sites.[11] Each BMG was prepared by the water-quenching technique to a size of 8–12 mm in diameter and 10–20 mm in length, where the melt was embedded in B_2O_3 solution during vitrification and was prevented from direct contact with the wall of the tube and the vacuum environment. The maximum diameter $d_{\max}$ of bulk samples of the individual alloy systems was determined. In the case of $Pd_{40}Cu_{40}P_{20}$, bulk samples could not be prepared. Instead, we produce a $Pd_{40}Cu_{40}P_{20}$ ribbon sample by a conventional melt-spinning technique with a B_2O_3 flux-treated master alloy. In addition, a $Pd_{40}Cu_{40}P_{20}$ plate of about 1-mm thick was prepared by the copper mold casting method. Induced coupling plasma (ICP) spectroscopy proved that the compositions of glass samples were in accordance with the nominal composition within an error of ± 0.4 at %. The amorphous nature of the glass was confirmed by x-ray diffraction analysis and optical microscopy. The specific heat curves of BMG and their crystallized counterparts were measured with a differential scanning calorimeter (DSC), a Perkin Elmer Pyris 1 DSC, and Diamond DSC under a pure Ar gas flow. Then the step-scan technique was employed with a temperature step of 10 K and time durations of 180–300 s as reported elsewhere.[3,14] The crystalline samples used were prepared by cooling a molten alloy up to ($T_m - 30$ K) for a week, followed by cooling it to room temperature. The weights of samples used ranged from 80 to 100 mg. The viscosities of $Pd_{46}Cu_{35.5}P_{18.5}$, $Pd_{40}Ni_{40}P_{20}$ (Ref. 15), $Pt_{60}Ni_{15}P_{20}$ (Ref. 15), and $Pd_{42.5}Cu_{30}Ni_{7.5}P_{20}$ (Ref. 15) BMG's were measured by isothermal creep experiments below T_g, followed by constant heating creep experiments with a rate of 0.083 K/s in a supercooled liquid region. The physical density of each sample was measured by the Archimedean method with *n*-Tridecane as a working fluid.

III. RESULTS

A. Thermodynamic properties of glass samples

The glass-forming range of the ternary Pd-Cu-P alloy was determined by He *et al.*[16] A representative $Pd_{40}Cu_{40}P_{20}$ alloy was reported to possibly form a bulk rod with a size of at least 7-mm diameter by the water-quenching method. However, we could not prepare any bulk-form glasses with this composition by the water-quenching method. The possibility may have been inferred from the fact that a master alloy was prepared differently from the literature.[16] Therefore, the optimized composition near $Pd_{40}Cu_{40}P_{20}$ was searched for and bulk-form glass with a composition of $Pd_{46}Cu_{35.5}P_{18.5}$ was found. The $d_{\max}$ of this glass reached approximately 12 mm. The thermodynamic properties of the glasses were examined by differential thermal analysis (DTA) conducted with a heating rate of 0.33 K/s. The DTA curves of BMG's as well as the ribbon-form $Pd_{40}Cu_{40}P_{20}$ prepared in the present work are shown in Fig. 1. The T_g, T_x, T_m, and T_l are summarized in Table I together with $d_{\max}$, T_{rg} and the γ parameter. Regarding $Pd_{40}Cu_{40}P_{20}$ glass, we assumed $d_{\max} \approx 2$ mm because the range $d_{\max} > 1$ mm can be deduced from the size of the sample produced by mold casting as mentioned in Sec. II. $Pd_{42.5}Cu_{30}Ni_{7.5}P_{20}$ glass[17] was obtained by further optimizing standard $Pd_{40}Cu_{30}Ni_{10}P_{20}$ glass with a $d_{\max}$ of 72 mm[9], and it is expected to show a larger $d_{\max}$ than $Pd_{40}Cu_{30}Ni_{10}P_{20}$ glass. However, we assumed, in this work, that the $d_{\max}$ of $Pd_{42.5}Cu_{30}Ni_{7.5}P_{20}$ glass is the same as that of $Pd_{40}Cu_{30}Ni_{10}P_{20}$ (i.e., $d_{\max} \approx 72$ mm). The $d_{\max}$ of $Pd_{40}Ni_{40}P_{20}$ glass has been improved[11,12,18] by means of the B_2O_3 flux treatment during the preparation of its master alloy and the quenching procedure. A value of $d_{\max} \approx 25$ mm is reported recently in Ref. 7, and it is much larger than expected from T_{rg} and the γ parameter. On the other hand, $Pd_{60}Ni_{15}P_{25}$ glass can be quenched in bulk form, $d_{\max} \approx 8$ mm, despite it having the lowest T_{rg} and smallest γ parameter among all the glasses prepared in the present work. The thermodynamic data of $Au_{76.9}Ge_{13.65}Si_{9.45}$[19,20] and $Pd_{77.5}Cu_6Si_{16.5}$[21,22] glasses are summarized in Table I for comparison, where $Au_{76.9}Ge_{13.65}Si_{9.45}$ glass with $d_{\max} \approx 0.04$ mm[20] was prepared by splat cooling. In the case of $Pd_{77.5}Cu_6Si_{16.5}$ glass, a variety of $d_{\max}$ values were reported and they corresponded to different types of vitrification methods. We adopted the maximum

TABLE I. Thermodynamic parameters of BMG's and ribbon-form $Pd_{40}Cu_{40}P_{20}$ glass. For comparison the data for $Pd_{77.5}Cu_6Si_{16.5}$[22] and $Au_{76.9}Ge_{13.65}Si_{9.45}$[20] glasses are indicated.

Glass	T_g [K]	T_x [K]	T_m [K]	T_l [K]	T_{rg}	γ	F_1	d_{max} [mm]	ΔH_m [J/mol]	ΔS_m [J/mol K]	a_0 [m]	V_M [m^3]
$Pd_{42.5}Cu_{30}Ni_{7.5}P_{20}$	571	640	795	828	0.690	0.458	0.546	≈72	6.37×10^3	8.01	0.257×10^{-9}	8.02×10^{-6}
$Pd_{43}Cu_{27}Ni_{10}P_{20}$	578	657	794	862	0.671	0.456	0.500	–	6.90	8.69	0.257	7.92
$Pd_{40}Ni_{40}P_{20}$	576	650	875	979	0.588	0.418	0.486	25	10.4	11.9	0.254	7.71
$Pd_{46}Cu_{35.5}P_{18.5}$	558	610	845	882	0.633	0.424	0.513	12	6.51	7.70	0.258	8.11
$Pt_{60}Ni_{15}P_{25}$	481	542	755	892	0.539	0.395	0.357	8	11.6	15.4	0.259	8.7
$Pd_{40}Cu_{40}P_{20}$	536	570	883	900	0.596	0.397	0.474[a]	≈2[b]	8.10	9.17	0.257	8.01
$Pd_{77.5}Cu_6Si_{16.5}$	639	672	1015	1036[c]	0.617	0.401	0.378	≈1[b]	7.25	7.15	0.268	8.67
$Au_{76.9}Ge_{13.65}Si_{9.45}$	295	300	625	650[c]	0.454	0.317	0.237	0.04[b]	10.6	17.0	0.277	10.6

[a]The viscosity of $Pd_{46}Cu_{35.5}P_{18.5}$ BMG is used (see the text) to calculate the F_1 parameter.
[b]Regarding the $Pd_{40}Cu_{40}P_{20}$ glass, d_{max} was deduced from a thickness ≈1 mm of plate-form glass. The $Pd_{77.5}Cu_6Si_{16.5}$ glass was prepared by directional solidification[21] and the $Au_{76.9}Ge_{13.65}Si_{9.45}$ glass[20] was made by splat cooling.
[c]The T_l was measured by the master alloy prepared in the present work.

size, $d_{max} \approx 1.0$ mm[21] among them, and it was obtained by directional solidification. Hereafter, in all the tables, the names of the glasses are arranged in the order of the magnitude of d_{max}.

B. Estimation of free-energy difference $\Delta G_{L-x}(T)$

The specific heats of the supercooled liquid, appearing after the glass transition on heating the glass solid, and the melt are plotted against temperature for individual molten alloys as well as their crystalline counterparts in Fig. 2. Hereafter, the results of each glass sample were represented by colored symbols and lines where black ($Pd_{42.5}Cu_{30}Ni_{7.5}P_{20}$), blue ($Pd_{43}Cu_{27}Ni_{10}P_{20}$), green ($Pd_{40}Ni_{40}P_{20}$), purple ($Pd_{46}Cu_{35.5}P_{18.5}$), red ($Pt_{60}Ni_{15}P_{25}$), and sky blue ($Pd_{40}Cu_{40}P_{20}$) were designated for six glass samples prepared in the present work. Pink and orange colors were used for the $Pd_{77.5}Cu_6Si_{16.5}$ and $Au_{76.9}Ge_{13.65}Si_{9.45}$ glass samples cited, respectively. The specific heat of the molten alloys was impossible to measure over the entire temperature range because of crystallization. Instead, the data of both supercooled liquid and equilibrium liquid were interpolated according to conventional Eq. (3) expressed as[5,23]

$$C_{P,L}(T) = 3R + aT + bT^{-2}, \tag{3}$$

where R is the gas constant. The specific heat data of the $Pd_{40}Ni_{40}P_{20}$ alloy have been reported by Kui and Turnbull[18] and are shown together with the results of the present work. Their specific heat curves seem to behave differently from

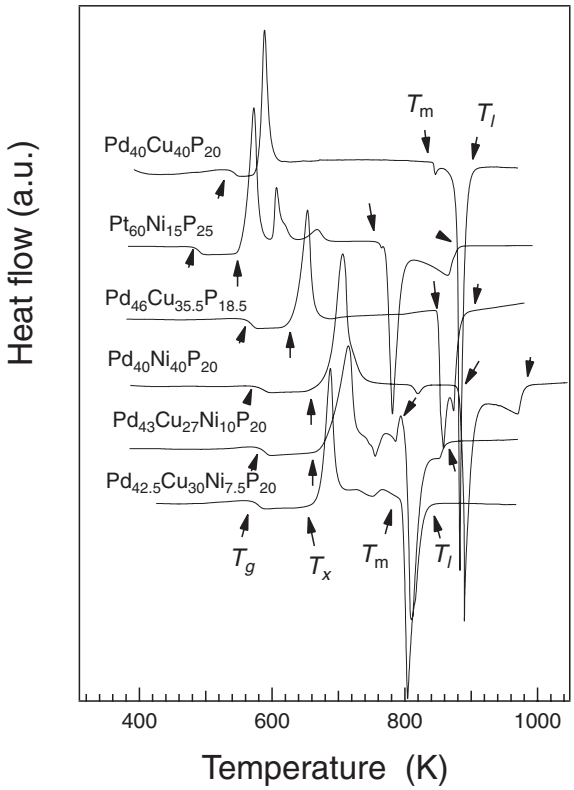

FIG. 1. DTA curves of BMG's and ribbon $Pd_{40}Cu_{40}P_{20}$ glass used in the present work. A heating rate of 0.33 K/s was employed.

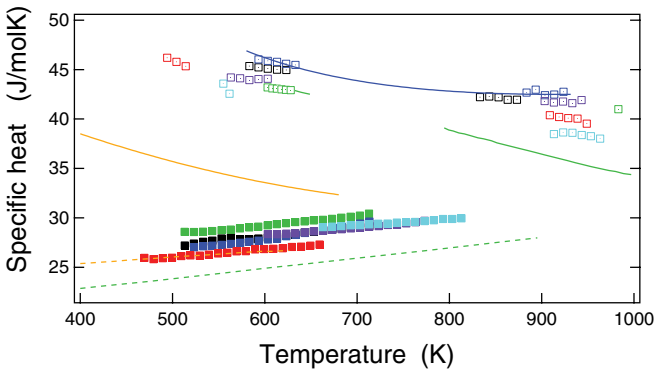

FIG. 2. (Color online) Specific heats $C_{P,L}(T)$ of liquids (open rectangles) and their crystalline counterparts (solid rectangles) $C_{P,x}(T)$ where each colored rectangle denotes $Pd_{42.5}Cu_{30}Ni_{7.5}P_{20}$ (black), $Pd_{43}Cu_{27}Ni_{10}P_{20}$ (blue), $Pd_{40}Ni_{40}P_{20}$ (green), $Pd_{46}Cu_{35.5}P_{18.5}$ (purple), $Pt_{60}Ni_{15}P_{25}$ (red), and $Pd_{40}Cu_{40}P_{20}$ (sky blue) alloy, respectively. The colored solid line corresponds to the specific heat curve of liquid against $Pd_{40}Ni_{40}P_{20}$ (measured[18]), $Pd_{43}Cu_{27}Ni_{10}P_{20}$ (calculated[5]), and $Au_{76.9}Ge_{13.65}Si_{9.45}$ (calculated[20]) alloys. The broken line corresponds to the specific curve of crystallized $Pd_{40}Ni_{40}P_{20}$ (measured[18]) and $Au_{76.9}Ge_{13.65}Si_{9.45}$ (measured[20]) alloys, respectively.

TABLE II. Parameters used to calculate $C_{P,L}(T)$ and $C_{P,x}(T)$ according to Eqs. (3) and (4).

Glass	a [J/mol K^2]	b [JK/mol]	c [J/mol K^2]	d [J/mol K^3]
$Pd_{42.5}Cu_{30}Ni_{7.5}P_{20}$	1.29×10^{-2}	4.50×10^{6}	1.42×10^{-3}	6.32×10^{-6}
$Pd_{43}Cu_{27}Ni_{10}P_{20}$	1.31	4.78	−3.78	14.4
$Pd_{40}Ni_{40}P_{20}$	1.28	3.76	4.86	3.78
$Pd_{46}Cu_{35.5}P_{18.5}$	1.33	3.85	3.43	3.37
$Pt_{60}Ni_{15}P_{25}$	1.15	3.82	−2.28	8.92
$Pd_{40}Cu_{40}P_{20}$	0.95	4.00	6.30	−0.204

those of other systems. Meanwhile, the specific curves in the present work do not deviate from those of other systems. However, owing to the limitation of temperatures available in an equilibrium liquid region ($T_l = 979$ K), a single value was measured at 983 K. We deduce that the discrepancy between the literature[18] and our work is caused by the difference between the experimental methods used (i.e., the continuous scan mode in the literature[18] and the step scan mode in the present work). Regarding $Pd_{43}Cu_{27}Ni_{10}P_{20}$ liquid, the present result is in good accordance with that reported in Ref. 5 (solid blue line). On the other hand, the specific heat of the crystal phase was best fitted by Eq. (4) as[5,23]

$$C_{P,x}(T) = 3R + cT + dT^2. \tag{4}$$

The coefficients a, b, c, and d are summarized in Table II for individual alloys, where in the case of $Pd_{77.5}Cu_6Si_{16.5}$ the specific heat difference $\Delta C_{P,L-x}(T) = C_{P,L}(T) - C_{P,x}(T) = 1.273 + 3.027 \times 10^{-14}T + 5.021 \times 10^{6}T^{-2}$ J/mol K was cited from the literature[21] instead of determined by independent calculation for individual $C_{P,L}(T)$ and $C_{P,x}(T)$. The free-energy difference $\Delta G_{L-x}(T)$ between the liquid and crystalline phases was calculated using $\Delta C_{P,L-x}(T)$ as

$$\Delta G_{L-x}(T) = (1 - T/T_m)\Delta H_m - \int_T^{T_m} \Delta C_{P,L-x} dT' + T \int_T^{T_m} \Delta C_{P,L-x}/T' dT', \tag{5}$$

where ΔH_m is the enthalpy of fusion presented in Table I together with the entropy of fusion $\Delta S_m = \Delta H_m / T_m$. The $\Delta G_{L-x}(T)$ curve was calculated as a function of the reduced temperature T/T_m and the result is shown in Fig. 3. With respect to $Pd_{40}Ni_{40}P_{20}$, two curves are drawn according to the results of the present work and in the literature[18] for comparison. We notice that the $\Delta G_{L-x}(T)$ curves of $Pd_{46}Cu_{35.5}P_{18.5}$ and quaternary Pd-Cu-Ni-P glasses show almost similar behaviors and they possess the lowest-energy difference (i.e., the smallest driving force to crystallization). On the other hand, $Pd_{40}Ni_{40}P_{20}$ and $Pt_{60}Ni_{15}P_{25}$ glasses exhibit fairly larger values than that of ribbon-form $Pd_{40}Cu_{40}P_{20}$ and $Pd_{77.5}Cu_6Si_{16.5}$ glasses with a lower GFA. This means that the GFA of Pd-P and Pt-P BMG's cannot be determined exclusively from the difference in $\Delta G_{L-x}(T)$, which is not in accordance with the prediction in the literature.[3–5]

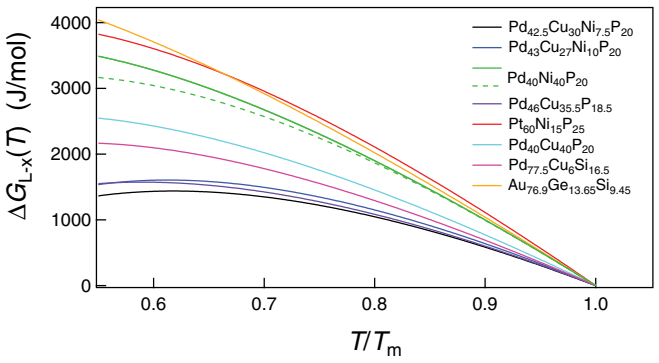

FIG. 3. (Color online) $\Delta G_{L-x}(T)$ of each BMG where, regarding $Pd_{77.5}Cu_6Si_{16.5}$ glass, it is cited from Ref. 21.

C. Viscosity of liquid

The viscosities measured were well fitted by the Vogel-Fulcher-Tammann formula as

$$\eta = \eta_0 \exp\left(\frac{D^* T_0}{T - T_0}\right), \tag{6}$$

where the fitted parameters η_0, D^*, and T_0 are summarized in Table III. We used the viscosity of $Pd_{43}Cu_{27}Ni_{10}P_{20}$ liquid reported in the literature,[24] which was analyzed using a cluster model. Figure 4 shows an Angell plot[25] of viscosity against temperature, where T_g^*'s are summarized in Table III. Since carrying out the viscosity experiments on the ribbon-form $Pd_{40}Cu_{40}P_{20}$ glass with the same accuracy as the bulk-form glasses was impossible, we substituted the viscosity of $Pd_{46}Cu_{35.5}P_{18.5}$ BMG for that of the ribbon-form $Pd_{40}Cu_{40}P_{20}$

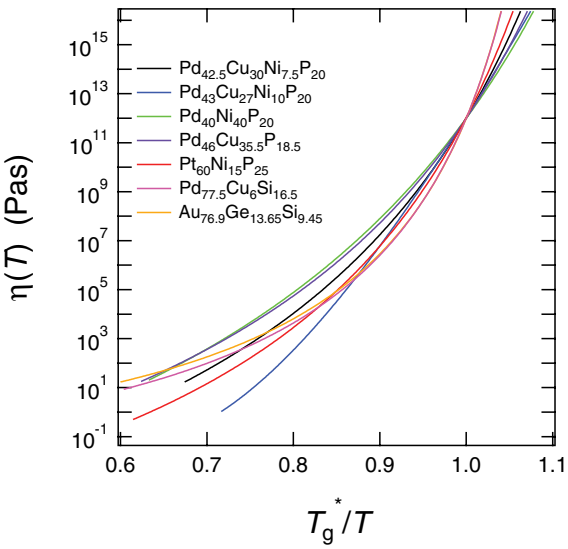

FIG. 4. (Color online) Angell plot of viscosity $\eta(T)$ against T_g^*/T.

TABLE III. Parameters obtained by fitting the viscosity date to Eq. (6) and T_g^* and m.

Glass	η_0 [Pa·s]	D^*	T_0 [K]	T_g^* [K]	m
$Pd_{42.5}Cu_{30}Ni_{7.5}P_{20}$	5.00×10^{-6}	16.5	379.0	536.0	59.1
$Pd_{43}Cu_{27}Ni_{10}P_{20}$ (Ref. 24)	–	–	–	569	65
$Pd_{40}Ni_{40}P_{20}$	5.30×10^{-6}	22.1	356.0	553.8	48.4
$Pd_{46}Cu_{35.5}P_{18.5}$	4.90×10^{-5}	17.0	362.6	527.0	52.3
$Pt_{60}Ni_{15}P_{25}$	4.50×10^{-6}	13.8	345.0	464.0	67.6
$Pd_{77.5}Cu_6Si_{16.5}$ (Ref. 19)	0.0152	6.20	513.0	613.0	84.7
$Au_{76.9}Ge_{13.65}Si_{9.45}$ (Ref. 20)	0.0520	5.64	241.3	285.8	85.4

glass. The identification of fragile and strong glass formers is generally performed using the fragility m, which was estimated according to Eq. (2) and summarized in Table III. $Pd_{40}Ni_{40}P_{20}$ glass was the strongest glass former among all the glasses used in the present work. Also, we can see that the fragility is not proportional to $d_{\max}$. The F_1 parameter was calculated using Eq. (1) with m and T_{rg} and the result is shown in Table I.

IV. DISCUSSION

From the results in the previous section, we can discuss the GFA of a glass system. Figure 5 shows plots of the logarithm of $d_{\max}$ against the T_{rg}, γ, or F_1 parameter. Although a moderate linear relation seems to be recognized from the relation of the logarithm of $d_{\max}$ versus γ, it seems to be poorly applicable to other parameters. Therefore, we search for another parameter that correlates to $d_{\max}$ from a fundamental aspect based on the thermodynamic consideration about the vitrification process. Following the classical nucleation theory (CNT), the steady-state homogeneous nucleation rate $I_{ss}(T)$ and the energy barrier of nucleation $\Delta G^*(T)$ are given by[26]

$$I_{ss}(T) = \frac{A}{\eta(T)} \exp(-\Delta G^*/k_B T), \quad A \approx \frac{N_A}{V_M} \cdot \frac{k_B T}{3\pi a_0^2}, \tag{7}$$

$$\Delta G^*(T) = 16\pi\sigma_{sL}^3/3[\Delta G_{L-x}(T)/V_M]^2, \tag{8}$$

where k_B is the Boltzmann's constant, N_A is the Avogadro's constant, and a_0 is the average atomic diameter calculated from the weighted sum r_G of Goldschmidt radii[27] for metallic elements and the atomic radius of P in tetrahedral covalent bonds. The a_0 values are summarized in Table I together with the molar volume V_M for each alloy crystal. $A \approx 10^{36}$ J/m^5 was obtained representatively at 600 K for all the glasses. $\Delta G^*(T)$ is the free-energy barrier between the liquid and the crystal to be surmounted to form a nucleus with a critical size $r^*(T)$ at a temperature T. It depends sensitively on the magnitude of the free-energy difference σ_{sL} at the nucleus-liquid interface as well as on $\Delta G_{L-x}(T)$.

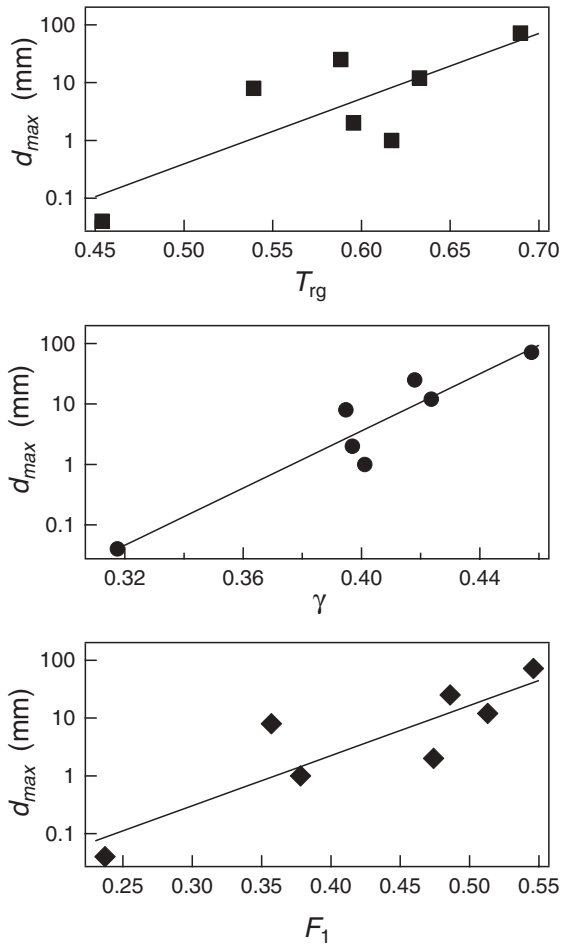

FIG. 5. Plots of $d_{\max}$ against T_{rg}, γ parameter and F_1 parameter.

A. Interfacial free energy between nucleus and liquid

Spaepen and Meyer[28] calculated the surface tension (i.e., interfacial free energy) of the crystal-liquid interface at the melting point T_m. They obtained $\sigma_g = \alpha_{fcc}\Delta h_m$, with $\alpha_{fcc} \approx 0.86$ for face-centered cubic (fcc) crystals, where σ_g and Δh_m are the tension and the heat of fusion per atom. Furthermore, on the basis of the statement by Miller and Chadwick[29] that the surface energy at T_m is higher than that obtained in an undercooled liquid, they proposed the temperature-dependent interfacial free energy $\sigma_{sL}(T)$ using the enthalpy of fusion ΔH_m rather than Δh_m as

$$\sigma_{sL}(T) = \frac{\alpha_{fcc}\Delta H_m}{\left(N_A V_M^2\right)^{1/3}} \cdot \frac{T}{T_m}. \tag{9}$$

α_{fcc} was later extended to include body-centered cubic (bcc) crystals by Thompson and coworkers[30,31] and it gave $\alpha_{bcc} = 0.71$. The crystallographic information on precipitates in $Pd_{40}Ni_{40}P_{20}$ and $Pd_{42.5}Cu_{30}Ni_{7.5}P_{20}$ glasses has been well examined. In $Pd_{40}Ni_{40}P_{20}$ glass[32], fcc-(Pd,Ni) solid solution, fcc-Pd_2Ni_2P, body-centered tetragonal (bct)-Ni_3P,

and orthorhombic crystals appeared after crystallization, and the precipitates of $Pd_{42.5}Cu_{30}Ni_{7.5}P_{20}$ glass[33] were composed of ordered Cu_3Au-type Cu_3Pd, $Cu_5Pd_3P_2$ (Pd_4Se-type simple tetragonal structure[34]), fcc-Pd_2Ni_2P and orthorhombic $Pd_{15}P_2$. According to the results of x-ray diffraction analysis, the Bragg peaks appearing in the crystallized $Pd_{46}Cu_{35.5}P_{18.5}$ alloy were mostly attributed to tetragonal $Cu_5Pd_3P_2$. However, it is possible that the diffraction peaks of any fcc-type crystals, as observed in the $Pd_{42.5}Cu_{30}Ni_{7.5}P_{20}$ alloy, are hidden in the diffraction pattern of the crystallized $Pd_{46}Cu_{35.5}P_{18.5}$ alloy. The precipitates in the crystallized $Pd_{77.5}Cu_6Si_{16.5}$[35] alloy are composed of an fcc-Pd solid solution and orthorhombic Pd_3Si. Regarding $Au_{76.9}Ge_{13.65}Si_{9.45}$ glass[20], fcc-gold and complex intermetallic compounds were reported as precipitates. The crystallographic data of crystal phases precipitated in $Pt_{60}Ni_{15}P_{25}$ glass seem to be nonavailable. Thus, we worked on $Pd_{40}Ni_{40}P_{20}$ BMG with the highest $T_m = 875$ K among the present BMG's to examine the effect of interfacial free energy on $I_{ss}(T)$. Kui *et al.* predicted[12] that the maximum value I_{ss}^{max} of a $Pd_{40}Ni_{40}P_{20}$ glass sufficiently treated with a B_2O_3 flux is less than 10^5 m^{-3} s^{-1}. Using Eqs. (6)–(9), $I_{ss}^{max} \approx 10^8$ m^{-3} s^{-1} ($\alpha_{bcc} = 0.71$) and $I_{ss}^{max} \approx 10^{-2}$ m^{-3} s^{-1} ($\alpha_{fcc} = 0.86$) were obtained. The calculation with α_{bcc} is close to that predicted in the literature, but is somewhat larger. Accordingly, we regarded α as an adjustable parameter to reproduce the I_{ss}^{max} predicted for $Pd_{40}Ni_{40}P_{20}$ glass and $\alpha \approx 0.76$ was determined. No bcc phase was reported in the $Pd_{40}Ni_{40}P_{20}$ alloy and more complex crystal structures were visualized. Although a complex crystal structure is expected to possess a smaller α than α_{bcc}, the previous result suggests that any crystal structure except fcc crystals can be approximated to have the same α as the bcc crystals. It is explained that the somewhat higher value $\alpha \approx 0.76$ may be caused by the precipitation of any fcc crystals. Eventually, throughout the present study, $\alpha \approx 0.76$ was used to evaluate the $I_{ss}(T)$ of glass systems except $Pt_{60}Ni_{15}P_{25}$ glass, whereas $\alpha_{bcc} = 0.71$ was applied only to this alloy because of the lack of reports on the precipitation of fcc crystals. The $\sigma_{sL}(T)$ curves are plotted against T/T_m in Fig. 6 for all the glasses together with $Pd_{77.5}Cu_6Si_{16.5}$ and $Au_{76.9}Ge_{13.65}Si_{9.45}$ glasses. Although $\sigma_{sL}(T)$ is very small for Pd-Cu-Ni-P_{20} glasses, they have a large d_{max} and are the best glass former in all the glasses investigated. This is due to the fact that $\Delta G_{L-x}(T)$ is also small for these alloy systems. We show the quantity $\Delta G^*(T)/k_BT$ at $T = T_{max}$ in the Table IV, where ΔG^* is the energy barrier height for the critical nucleus formation and T_{max} is the temperature that gives the maximum value of $I_{ss}(T)$. $\Delta G^*(T)/k_BT_{max}$ is largest, 60.0, for two quaternary Pd-P-based glasses among all the glasses. As given in Eq. (8), $\Delta G^*(T)$ is determined by the competition between $\sigma_{sL}(T)$ and $\Delta G_{L-x}(T)$. Therefore, we conclude that the smallness of $\sigma_{sL}(T)$ does not decisively influence the degradation of GFA as seen for these glass systems.

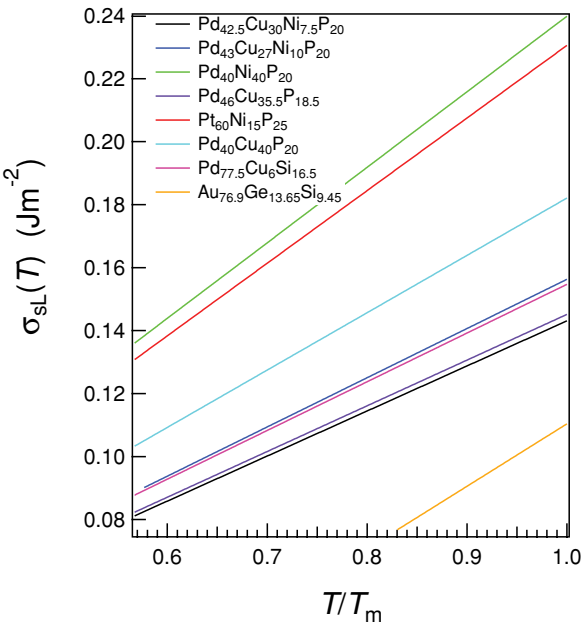

FIG. 6. (Color online) Interfacial free-energy curves $\sigma_{sL}(T)$ illustrated as functions of T/T_m.

Although the available calculation of σ_{sL} is, so far, limited to fcc and bcc crystal structures, its application to the hexagonal closed packed (hcp) crystal structure may be physically acceptable because of the same atomic packing fraction as the fcc crystal structure, and it gives the result $\alpha_{hcp} = \alpha_{fcc}$. With respect to other crystalline systems, we approximated their α's as 0.71 (the same as α_{bcc}). This will somewhat oversimplify the actual α's of any complex crystallize phases, which are expected to be smaller than α_{bcc}. Therefore, the estimation of σ_{sL} gave an upper limit to the actual value, in the present study, and it resulted in an under limit of $I_{ss}(T)$ calculated.

TABLE IV. The maximum energy barrier $\Delta G^*_{max}/k_B \cdot T_{max}$ for the formation of a critical nucleus and the maximum nucleation rate I_{ss}^{max} together with t_n, T_n, and R_c^h.

Glass	T_{max} [K]	$\Delta G^*_{max}/k_B \cdot T_{max}$	I_{ss}^{max} [m^{-3} s^{-1}]	T_n [K]	t_n [s]	R_c^h [Ks^{-1}]
$Pd_{42.5}Cu_{30}Ni_{7.5}P_{20}$	517	60.0	1.27×10^{-4}	568	9.03×10^{9}	2.51×10^{-8}
$Pd_{43}Cu_{27}Ni_{10}P_{20}$	510	60.0	5.26×10^{-9}	578	2.10×10^{13}	–
$Pd_{40}Ni_{40}P_{20}$	525	38.1	1.18×10^{5}	591	7.41×10^{7}	3.83×10^{-6}
$Pd_{46}Cu_{35.5}P_{18.5}$	526	46.3	2.70×10^{4}	584	4.38×10^{6}	5.95×10^{-5}
$Pt_{60}Ni_{15}P_{25}$	459	53.3	5.90×10^{4}	510	2.66×10^{6}	9.20×10^{-5}
$Pd_{40}Cu_{40}P_{20}$	531	32.8	4.88×10^{10}	597	3.74×10^{4}	7.60×10^{-3}
$Pd_{77.5}Cu_6Si_{16.5}$	642	32.7	2.68×10^{13}	700	245	1.30
$Au_{76.9}Ge_{13.65}Si_{9.45}$	317	25.7	1.85×10^{19}	356	0.451	596

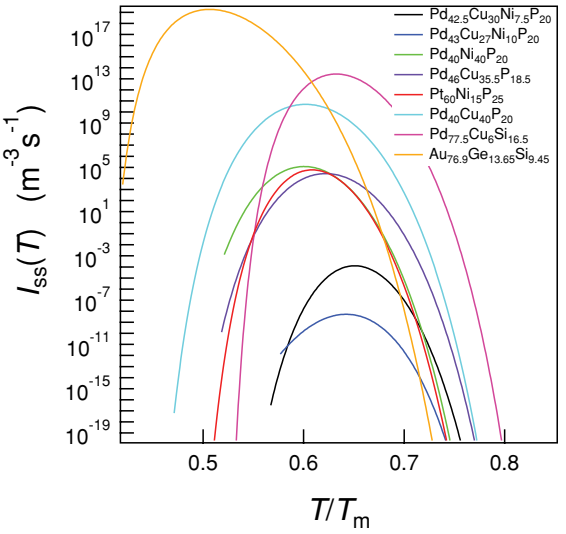

FIG. 7. (Color online) Plot of homogeneous steady-state nucleation rate $I_{ss}(T)$ against T/T_m.

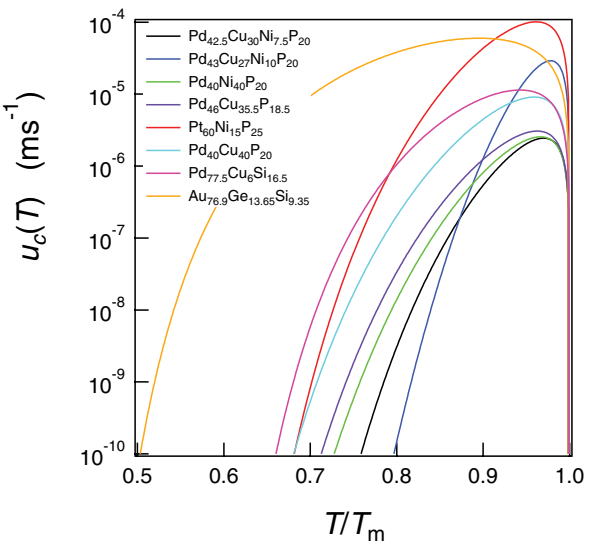

FIG. 8. (Color online) Plot of growth rate $u_c(T)$ against T/T_m.

B. $I_{SS}(T)$, $u_c(T)$ and R_c^h

First, we examine the validity of CNT against the present work. According to Eqs. (5) and (9), we can calculate the critical size $r^*(T_n) = 2\sigma_{sL}(T_n)V_M/\Delta G_{L-x}(T_n)$ of cluster nuclei and the number $N_c(T_n) \approx (r^*/r_G)^3$ of atoms in the cluster at the temperature. The $r^*(T_n)$ values ranged from 0.58 ($Au_{76.9}Ge_{13.65}Si_{9.45}$) to 1.2 nm ($Pd_{42.5}Cu_{30}Ni_{7.5}P_{20}$) and they corresponded to $N_c(T_n) \approx 70$ and $N_c(T_n) \approx 800$ atoms, respectively. Trudu *et al.*[36] concluded from their computer simulation results that the crystallization process in a deep undercooled region could be controlled by a spinodal decomposition process due to the instability of the liquid phase instead of by a traditional nucleation and growth process because the density fluctuation in a liquid induces the spontaneous formation of the nucleus when the cluster size becomes much smaller. On the basis of this concept, Leyssale *et al.*[37] examined the validity of CNT to explain the kinematical behavior of nucleus formation and its morphology. They reported that the computer simulation result is consistent with the result obtained using CNT down to the size of a nucleus with about 40 molecules. The smallest number, $N_c(T_n) \approx 70$, of atoms for $Au_{76.9}Ge_{13.65}Si_{9.45}$ glass in the present work is larger than the critical number predicted. Thus we conclude that CNT analysis is suitable for discussing the thermodynamic stability of molten alloys prepared with B_2O_3 flux.

The I_{ss} (T) curves calculated are presented as functions of T/T_m in Fig. 7. They are classified roughly into three groups: (a) $Pt_{60}Ni_{15}P_{25}$ and $Pd_{46}Cu_{35.5}P_{18.5}$ glasses have compatible I_{ss}^{max} with $Pd_{40}Ni_{40}P_{20}$ glass; (b) the I_{ss}^{max} of $Pd_{40}Cu_{40}P_{20}$ glass is much larger than that of $Pd_{40}Ni_{40}P_{20}$ glass and compatible with those of $Pd_{77.5}Cu_6Si_{16.5}$ and $Au_{76.9}Ge_{13.65}Si_{9.45}$ glasses; and (c) I_{ss}^{max} values are extremely small for quaternary Pd-P-based glasses (i.e., only on the order of magnitude of 10^{-4} to 10^{-9} $m^{-3}\,s^{-1}$). These values are much smaller than $I_{ss}^{max} \approx 10^5$ $m^{-3}\,s^{-1}$ calculated for $Pd_{40}Cu_{30}Ni_{10}P_{20}$ glass[38] with a semiempirical expression of $\Delta G^*(T)$. The $\Delta G^*_{max}/k_B \cdot T_{max}$ values are summarized in Table IV together with I_{ss}^{max}, where T_{max} denotes the temperature that gives I_{ss}^{max}.

We notice that both I_{ss}^{max} and ΔG^*_{max} cannot reproduce well the sequence of the magnitude of d_{max}.

It is evident that a nucleus with a remarkable low growth rate cannot develop in size. Therefore, it is important to examine the growth rate $u_c(T)$ as well as $I_{ss}(T)$ during the vitrification of molten alloys. Equation (10) gives the steady-state growth rate[27] of the nucleus as a function of temperature

$$u_c(T) = f\frac{D}{a_0}\left[1 - \exp\left(-\frac{\Delta G_{L-x}}{RT}\right)\right], \quad D = \frac{k_B T}{3\pi a_0 \eta(T)}, \tag{10}$$

where the coefficient f is approximately given[28] as $f \approx 0.2(T_m - T)/T_m$ under the condition $\Delta S_m < 2R$. As seen in Table I, this constraint was satisfied for all the alloy systems. Using $\Delta G_{L-x}(T)$ and $\eta(T)$, $u_c(T)$ was calculated and the result is illustrated in Fig. 8. The u_c^{max} values ranged from 10^{-6} to 10^{-4} ms^{-1} among the present alloy systems. The smallest u_c^{max} is realized in $Pd_{42.5}Cu_{30}Ni_{7.5}P_{20}$ glass, but it is much larger than $u_c^{max} \approx 5 \times 10^{-9}$ ms^{-1} obtained empirically for $Pd_{40}Cu_{30}Ni_{10}P_{20}$ glass.[38] We readily notice that the $u_c(T)$ of $Pt_{60}Ni_{15}P_{25}$ glass takes large values over a wide temperature range. This means that the introduction of a small number of crystalline embryos and/or heterogeneous nucleation sites would promote the rapid growth of the crystal phase because this system inherently possesses a smaller I_{ss}^{max}, comparable with that of $Pd_{40}Ni_{40}P_{20}$ glass, as seen in Fig. 7. The u_c of $Pd_{43}Cu_{27}Ni_{10}P_{20}$ glass was relatively large in the vicinity of T_m, but it became smallest at approximately T_g and such a feature may be based on a peculiar temperature dependence of viscosity, as will be mentioned later. Drehman and Greer[11] measured the maximum steady-state nucleation rate I_{ss}^{max}, an order of magnitude of 10^4–10^6 $m^{-3}\,s^{-1}$ for $Pd_{40}Ni_{40}P_{20}$ glass. On the basis of this value, they derived $u_c^{max} \approx 10^{-10}$ ms^{-1}. In the present work, u_c was calculated using only experimental values for ΔG_{L-x} and η in Eq. (10), and eventually $u_c^{max} \approx 10^{-6}$ ms^{-1} was obtained as shown in Fig. 8. Accordingly, $u_c^{max} \approx 10^{-10}$ ms^{-1} in the literature[12] seems to be much smaller than that in the present work. Nishiyama and Inoue[9] measured $u_c \approx 3.2 \times 10^{-7}$ ms^{-1} from

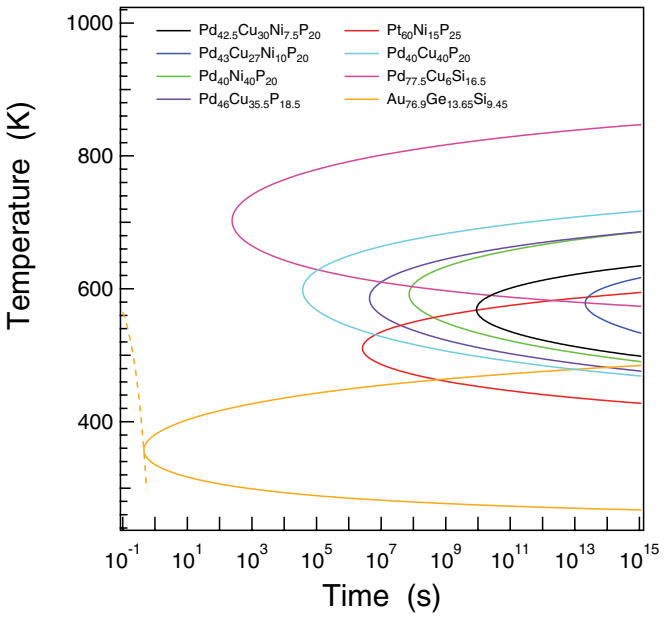

FIG. 9. (Color online) TTT diagram calculated using $I_{ss}(T)$ and $u_c(T)$ together with the cooling curve of $Au_{76.9}Ge_{13.65}Si_{9.45}$ melt.

the optical observation of a cross section of $Pd_{42.5}Cu_{30}Ni_{7.5}P_{20}$ glass partially devitrified at 683 K, which is slightly higher than T_x. This value is compatible with the present result (i.e., $u_c \approx 1.1 \times 10^{-7}$ ms^{-1} at 683 K). Also, it is evident that $u_c^{\max}$ is not in agreement with the sequence of the magnitude of $d_{\max}$.

Using $I_{ss}(T)$ and $u_c(T)$, we can evaluate the critical cooling rate R_c^h through the equation[39] $X(t) \approx \frac{1}{3}\pi I_{ss}(T) u_c^3(T) t^4$, where $X(t)$ denotes the crystallized fraction at time t. The temperature-time-transformation (TTT) curve was derived with $X = 10^{-6}$ and the result is shown in Fig. 9. To estimate R_c^h, the cooling curve of a liquid was drawn in the figure, as illustrated representatively for $Au_{76.9}Ge_{13.65}Si_{9.45}$ glass. The contact of the cooling curve with the nose of the TTT curve gave the time $t_n = 0.45$ s and the temperature $T_n = 357$ K and we could estimate $R_c^h = (T_m - T_n)/t_n \approx 6.0 \times 10^2$ Ks^{-1} for this case. Such an estimate was performed similarly for other glass systems, and the R_c^h values obtained are summarized in Table IV together with t_n and T_n. The relationship

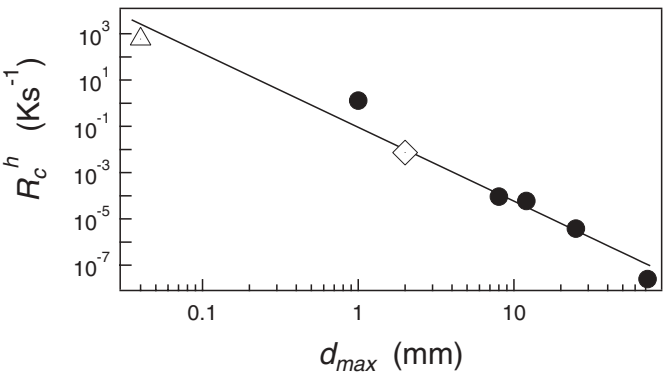

FIG. 10. Plot of critical cooling rate R_c^h against $d_{\max}$. Solid circles denote the data obtained from the present work and open triangle and diamond represent $Au_{76.9}Ge_{13.65}Si_{9.45}$ and $Pd_{77.5}Cu_6Si_{16.5}$ glass, respectively.

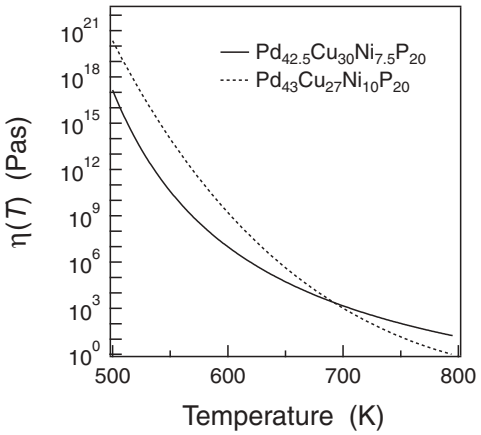

FIG. 11. Comparison of the $\eta(T)$ curve of $Pd_{42.5}Cu_{30}Ni_{7.5}P_{20}$ glass with that of $Pd_{43}Cu_{27}Ni_{10}P_{20}$ glass.

between R_c^h and $d_{\max}$ is plotted in Fig. 10 and is well described by

$$\log_{10}\left(R_c^h\right) = (-3.2 \pm 0.3)\log_{10}(d_{\max}) - 1.0 \pm 0.3. \quad (11)$$

We can see a distinct linear relation between $\log_{10}(R_c^h)$ and $\log_{10}(d_{\max})$ (i.e., roughly $R_c^h \approx d_{\max}^{-3}/10$ mm^3 Ks^{-1}). Kiminami and Sahm[22] concluded that the vitrification process of $Pd_{77.5}Cu_{6.0}Si_{16.5}$ glass is predominantly controlled by a homogeneous nucleation and growth mechanism. The present result indicates the validity of their conclusion. A similar consideration will be true for $Au_{76.9}Ge_{13.65}Si_{9.45}$ glass made by the splat cooling method.[19]

In the present study, a $Pd_{43}Cu_{27}Ni_{10}P_{20}$ glass showed the smallest R_c^h, and $d_{\max}$ will be the largest of all the glasses examined, although it is actually unverified. The conclusion is mostly attributed to the smallest $I_{ss}^{\max}$ of this glassy system. As shown in Table IV, the $\Delta G^*_{\max}/k_B \cdot T_{\max}$ values are the same for both $Pd_{43}Cu_{27}Ni_{10}P_{20}$ and $Pd_{42.5}Cu_{30}Ni_{7.5}P_{20}$ glasses at $T_{\max}$. As a consequence, the difference in $I_{ss}^{\max}$ is ascribed to the difference in the viscosity. The viscosity curves of both glasses are shown as functions of temperature in Fig. 11. The viscosity of $Pd_{43}Cu_{27}Ni_{10}P_{20}$ glass is larger by an order of magnitude of 10^3 Pa·s at approximately $T_g \approx 570$ K than $Pd_{42.5}Cu_{30}Ni_{7.5}P_{20}$ glass. Although Kato *et al.*[15] and Fan *et al.*[24] employed different methods to measure viscosity, thermal conditions applied to both glass systems were then mostly similar. It is difficult for us to strictly control the composition of any Pd-Cu-Ni-P alloy because of the high vapor pressure and low melting temperature of P atoms and the easy formation of P oxides. It is possible that the two glass systems possess a larger fluctuation in local composition or topological disorder than expected from the difference in their nominal compositions, which affected the behavior of the viscosity at approximately T_g.

V. CONCLUSION

To elucidate the GFA of water-quenched BMG's such as ternary $Pd_{40}Ni_{40}P_{20}$, $Pd_{46}Cu_{35.5}P_{18.5}$, $Pt_{60}Ni_{15}P_{25}$ and quaternary $Pd_{43}Cu_{27}Ni_{10}P_{20}$, $Pd_{42.5}Cu_{30}Ni_{7.5}P_{20}$ as well as melt-spun $Pd_{40}Cu_{40}P_{20}$ ribbons, the validity of the thermodynamic approach in terms of the CNT was examined. The

water-quenched BMG's used in this work were sufficiently treated with a dehydrated B_2O_3 flux prior to and while quenching the melt so that the heterogeneous nucleation and growth sites were mostly removed from the melts. Accordingly, the vitrification process was dominated by a homogenous nucleation and growth mechanism. No available parameter such as such as the T_{rg}, γ parameter or F_1 parameter reproduced the sequence of the magnitude of d_{max} experimentally obtained. Similarly, individual thermodynamic quantities such as I_{ss}^{max}, u_c^{max}, ΔG_{max}^*, ΔG_{L-x}, and σ_{sL} were useless to interpret the sequence of the magnitude of d_{max}. The only strong correlation appeared in the relation between $\log_{10}(R_c^h)$ and $\log_{10}(d_{max})$, roughly $R_c^h \approx d_{max}^{-3}/10\ \text{mm}^3\ \text{Ks}^{-1}$, where the critical cooling rate R_c^h was estimated from the cooling curve of the melt and the TTT curve calculated by taking account of the homogeneous nucleation theory on the vitrification of molten alloys. We conclude that the GFA of a glass system should be estimated in terms of the "ideal" critical cooling rate calculated from the homogeneous steady-state nucleation and growth because it is an intrinsic property of individual alloy systems.

ACKNOWLEDGMENT

We would like to thank Y. Yokoyama for preparing the plate-form $Pd_{40}Cu_{40}P_{20}$ glass.

[1]Z. P. Lu and C. T. Liu, Acta. Mater. **50**, 3501 (2002).
[2]O. N. Senkov, Phys. Rev. B **76**, 104202 (2007).
[3]R. Busch, W. Liu, and W. L. Johnson, J. Appl. Phys. **83**, 4134 (1998).
[4]Q. K. Jiang, X. D. Wang, X. P. Nie, G. Q. Zhang, H. Ma, H.-J. Fecht, J. Bendnarcik, H. Franz, Y. G. Liu, Q. P. Gao, and J. Z. Jiang, Acta Mater. **56**, 1785 (2008).
[5]G. J. Fan, J. F. Löffler, R. K. Wunderlich, and H.-J. Fecht, Acta Mater. **52**, 667 (2004).
[6]N. Nishiyama and A. Inoue, Mater. Trans. **43**, 1247 (2002).
[7]T. D. Shen and R. B. Schwarz, Appl. Phys. Lett. **88**, 091903 (2006).
[8]Y. He, R. B. Schwarz, and J. I. Archuleta, Appl. Phys. Lett. **69**, 1861 (1996).
[9]N. Nishiyama and A. Inoue, Mater. Trans., JIM **38**, 464 (1997).
[10]J. Schroers and W. L. Johnson, Phys. Rev. Lett. **93**, 255506 (2004).
[11]A. J. Drehman and A. L. Greer, Acta Metall. **32**, 323 (1984).
[12]H. W. Kui, A. L. Greer, and D. Turnbull, Appl. Phys. Lett. **45**, 615 (1984).
[13]Y. Q. Cheng, H. W. Sheng, and E. Ma, Phys. Rev. B **78**, 014207 (2008).
[14]H.-J. Fecht, J. H. Perepezko, M. C. Lee, and W. L. Johnson, J. Appl. Phys. **68**, 4494 (1990).
[15]H. Kato, T. Wada, M. Hasegawa, J. Saida, A. Inoue, and H. S. Chen, Scr. Mater. **54**, 2023 (2006).
[16]Y. He, T. Shen, and R. B. Schwarz, Metall. Mater. Trans. A **29**, 1795 (1998).
[17]N. Nishiyama and A. Inoue, Appl. Phys. Lett. **80**, 568 (2002).
[18]H.-W. Kui and D. Turnbull, J. Non-Cryst. Solids **94**, 62 (1987).
[19]H. S. Chen and D. Turnbull, Appl. Phys. Lett. **10**, 284 (1967).
[20]H. S. Chen and D. Turnbull, J. Chem. Phys. **48**, 2560 (1968).
[21]F. Gillessen and D. M. Herlach, J. Non-Cryst. Solids **117**/**118**, 555 (1990).
[22]C. S. Kiminami and P. R. Sahm, Acta Metall. **34**, 2129 (1986).
[23]R. Busch, Y. J. Kim, and W. L. Johnson, J. Appl. Phys. **77**, 4039 (1995).
[24]G. J. Fan, H.-J. Fecht, and E. J. Lavernia, Appl. Phys. Lett. **84**, 487 (2004).
[25]C. A. Angell, J. Non-Cryst. Solids **13**, 131 (1991).
[26]D. H. Herlach, Mater. Sci. Eng., R **12**, 177 (1994).
[27]C. Kittel, in *Introduction to Solid State Physics* (John Wiley & Sons, New York, 2005), p. 71.
[28]F. Spaepen and R. B. Meyer, Scr. Metall. **10**, 257 (1976).
[29]W. A. Miller and G. A. Chadwick, Acta Metall. **15**, 607 (1967).
[30]C. V. Thompson, Ph.D., Harvard University, 1981.
[31]C. V. Thompson and F. Spaepen, Acta Metall. **31**, 2021 (1983).
[32]J. Z. Jiang, K. Saksl, N. Nishiyama, and A. Inoue, J. Appl. Phys. **92**, 3651 (2002).
[33]C. Ma, N. Nishiyama, and A. Inoue, Mater. Trans. **43**, 1161 (2002).
[34]M. EI-Boragy, M. Ellner, and K. Schubert, Z. Metall. Bd. **75**, 302 (1984).
[35]P. G. Boswell and G. A. Chadwick, Scr. Metall. **10**, 509 (1976).
[36]F. Trudu, D. Donadio, and M. Parrinello, Phys. Rev. Lett. **97**, 105701 (2006).
[37]J.-M. Leyssale, J. Delhommelle, and C. Millot, J. Chem. Phys. **127**, 044504 (2007).
[38]N. Nishiyama and A. Inoue, Acta Mater. **47**, 1487 (1999).
[39]D. R. Uhlmann, J. Non-Cryst. Solids **7**, 337 (1972).